A Case Study of 3D geomodelling of Frontier Formation Second Wall Creek Sand, Teapot Dome, Wyoming, USA

Haris Ahmed Khan*[1], Masood Sultan[2], Muhammad Jahangir Khan[1], Maria Dolores Alvarez[3], Syed Danial Mehdi[1] and Muhammad Aqib Javed[1]

1. Department of Earth and Environmental Sciences, Bahria University, Karachi Campus, 13 National Stadium Road, Karachi 75260, Pakistan.
2. Institute der Mathematisch- Naturwissenschaftlichen Fakultät, Institut für Geographie, Geographisches Institut, Humboldt University zu Berlin, Rudower Chaussee 16. 12489 Berlin.
3. Argentina's Geological and Mining Survey, Aveneida General Paz 5445 – Edificio 25 – INTI – General San Martin – Argentina.

Correspondence: haris.bukc@bahria.edu.pk,
haris_geologist@hotmail.com.
ORCIDs: https://orcid.org/0000-0001-2345-6789

Correspondence Email Addresses

Haris Ahmed Khan	: haris.bukc@bahria.edu.pk
Masood Sultan	: masood.geo@yahoo.com
Muhammad Jahangir Khan	: mjahangir.bukc@bahria.edu.pk
Maria Dolores Alvarez	: dolores.alvarez@segemar.gov.ar
Syed Danial Mehdi	: mehdi.geophysicist@gmail.com
Muhammad Aqib Javed	: aqib_geoscientist@outlook.com

1. Introduction

The study area lies in the Powder River Basin (PRB) which is an elongated north-south trending asymmetrical basin spreading over 22,000 square miles (Payne and Saffer, 2005). PRB is one of the largest producing basins within the United States of America, with 2.3 TCF gas and more than 2.7 billion barrels of recoverable oil has been discovered within the basin following the Salt Creek exploration in 1908 (Curry Jr, 1977). The basin comprises around 700 fields in which 225 are of a magnitude greater than 1 MMBOE (Dolton and Fox, 1995). The western limb of the basin is dipping enough to overturn the rocks to the east while the eastern limb has a gentle dip from the western edge of the Black Hills (Fig. 1). The basin was a part of relatively stable interior platform which was flooded by epicontinental seas depositing the carbonates and the clastic sediments in cyclic sea-level rise and falls during Cambrian to Cretaceous (Beikman, 1962). The PRB lies in the states of Wyoming (with a covered area of 75%) and Montana (25% of the area). (Fig. 1a).

The Teapot Dome is located within the PRB which is an elongated asymmetrical, doubly plunging, Laramide age anticline spanning a near area of 9481 acres consisting of Teapot Dome and Salt Creek oil fields being separated by NE-SW oblique fault. The Teapot Dome is situated in the central Wyoming near the southwestern edge of the PRB (Cooper et al., 2006), it is bounded from west by the Casper arch, PRB to the east, in the South with Laramie Uplift (Fig. 1) and Owl Creek Uplift to the North.

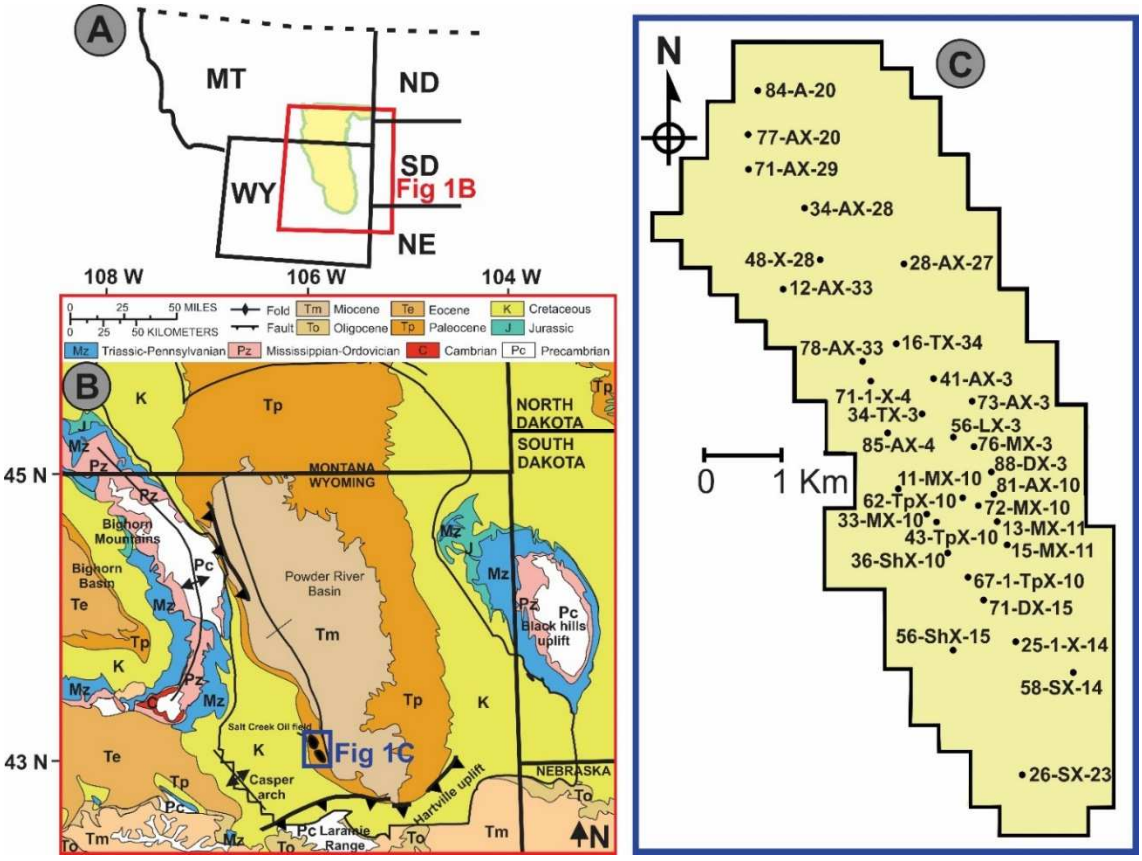

Figure 1: (A) Location of PRB in USA. (B) Geological map of PRB and surrounding Laramide uplifts modified: (Craddock et al., 2012). (C) Boundary of Teapot Dome represented by solid black line (shown by the step stair pattern), well locations by black dots.

1.1. GEOLOGY OF THE AREA

1.1.1 Basin Tectonostratigraphy

The understudy basin is composed of Precambrian to recent formations that account to a total thickness of 17,000 feet (Love et al., 1993). The Precambrian rocks are exposed in the adjacent mountain ranges of the Black hills uplift and the Bighorn (Houston, 1993). From Cambrian to Mississippian the deposition followed the shallow marine deposits (Fig. 2), it is one of the widespread deposits during the Paleozoic (Craig et al., 1979). The uplift of Rocky Mountains introduced a new sequence of deposits, the Tensleep

Sandstone and equivalents were deposited from the erosion of the ancestral Rocky Mountains (Love et al., 1993). The Permian observed an alternating shallow marine to continental and vice versa depositional environment, that resulted in the shale, limestone and anhydrites of the Goose Egg Formation. The fluctuations of the western margin of North America dominated the oscillations in the northeastern Wyoming during the start of Mesozoic Era. The shelf of the Wyoming was uplifted during the Triassic and resulted in the deposition of the terrestrial beds of evaporites (Picard et al., 1993). In the Jurassic the shelf kept subducting and rising which caused the transgressive and regressive shale-sand deposits (Picard et al., 1993). In the latter part of Jurassic the shelf was uplifted and dominated by the terrestrial deposits consisting of shale interbedded with sandstone, siltstone, and conglomerate deposited on the alluvial plain (Watson, 1980). Western Interior Seaway was developed from the Gulf of Mexico to the Arctic Ocean which deposited thousands of feet of sedimentary rocks through the transgressive and regressive cycles (Peterson, 1972). The first major transgressive deposit of Fall River Sandstone and the Thermopolis Shale were deposited on the marginal marine environment with a regressive deposition of the Carlile, Niobrara, and Steele shale.

The Paleocene series consists of Fort Union Formation which is composed of Sandstone, conglomerate, shale and coal which was deposited with fluvial systems on the flood plains and peat swamps (Watson, 1980). During the Eocene and Oligocene, the deposits consisted of volcanic ash and alluvial deposits which resulted from the closure of the Western Interior Seaway followed by the Cretaceous uplift.

The present-day Wyoming along with much of the Rocky Mountain west were located on a stable continental shelf (Lageson and Spearing, 1991). It was covered by shallow sea, with fluctuations in the sea level aggradation, transgressional and regression layers of sediments were deposited, these changes also resulted in unconformities due to erosion (Fig. 2).

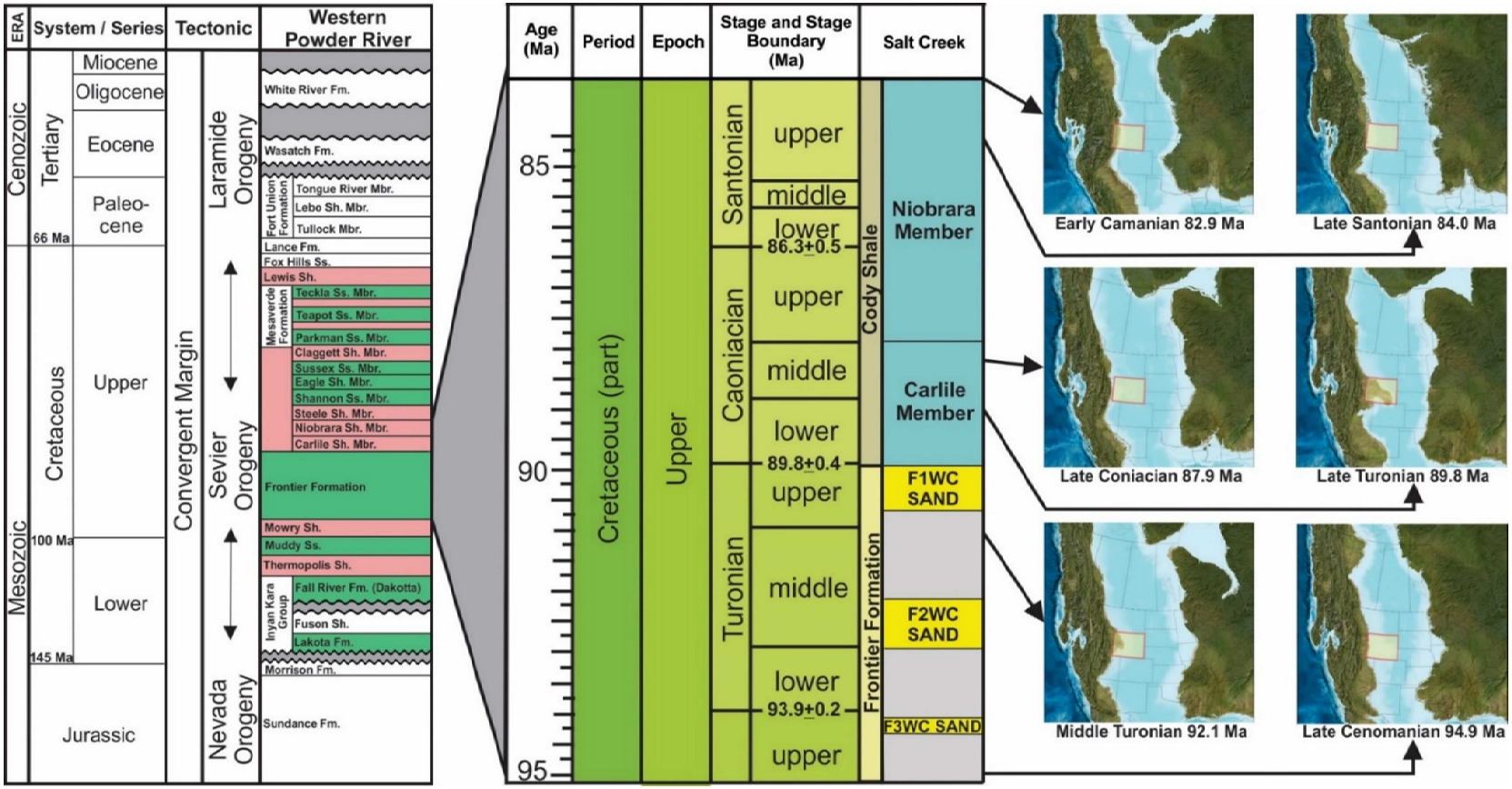

Figure 1: Tectonostratigraphic chart of Powder River Basin from Jurassic to Miocene, modified: (Craddock et al., 2012), with paleogeographic dynamics of Cretaceous Western Interior Seaway, modified: (Blakey, 2014). The Cretaceous period from 95 to 84 Ma has been exaggerated and each formation from F3WC to Niobrara Shales has been further described as of Late Cenomanian to Late Santonian respectively. Each paleogeographic image represents the boundary of Wyoming in yellow box bounded by red border.

The mature organic rich rocks of the upper Cretaceous Carlile and Niobrara are the primary source of oil found in the Frontier Play, they contain a mixture of type II and III organic matter. Along with the overlying sources, the interbedded shales of the regressive phase within the deposition cycle of Frontier Formation also charge the reservoir.

During the phase of Laramide orogeny the hydrocarbon generation and migration is expected to have happened, the faulting also helped in the maturation and migration phase. The play consists of relatively high API gravity oil ranging from 34 to 47 API (Dolton and Fox, 1995). The Frontier Sandstone play is a stratigraphic trap in offshore marine shelf sandstones of the Cretaceous large and high-energy bar complexes. The sandstone is a bioturbated shoreface deposit of the Late Cretaceous around 83.5 Ma ago which was resulted during the Western Interior Seaway Regression (Walker and Bergman, 1993; Tillman and Martisen, 1984). The play is a part of the prograding clastic sequence which was derived from the erosion of western Rocky Mountains (Walker and Bergman, 1993). As the play is a stratigraphic trap on the regional scale, the hydrocarbon accumulation is greater on the pinchout and complex margins, while at the Teapot the anticline structure caused the accumulation within the domal 3D closure by the shales of Niobrara and Carlile (Association, 2000).

2. DATASET AND METHODOLOGY

The analyses and interpretation of geophysical data consisting of 32 wells and 3D seismic volume (345 In Lines and 118 X Lines) spanning over 3 seconds and spatial seismic coverage about 40 km^2 was performed in the study. The petrophysical logs including Gamma Ray (GR), Sonic (DT), Neutron porosity (NPHI), Density (RHOB),

Resistivity (LLD, LLS, and MSFL) were utilized to estimate the reservoir characteristics (volume of shale, porosity, permeability, saturation of water). The provided seismic data is 3D post-stack time migrated and in Segy format characterized with a Seismic Reference Datum at 5500 ft and a replacement velocity of 9000 ft/sec which we have visualized and interpreted for detailed analysis of the study area. The interpretation of the Frontier Formation Second Wall Creek (F2WC) Sand interval (horizons) over seismic profiles to understand the reservoir distribution in the study area by depth modelling followed by synthetic seismogram generation were a major part of the study. For the characterization of sand facies, the integration of seismic, well log and geostatistical analyses has been completed which manifest 3D models of F2WC in the Teapot Dome.

3. RESULTS AND DISCUSSION

The results of this study classified into three parts 1) Well logs analysis 2) Basic seismic interpretation and modelling 3) 3D geostatistical analysis.

3.1. Well Log Analysis

The well log analysis begins with lithology interpretation mainly based on GR and supported by NPHI and RHOB logs. We have classified the alternate facies of sand and shale deposited in upper Cenomanian to Turonian (Frontier formation) by using the GR cut-off ratios (Table 1) which validated the cross plots (available NPHI-RHOB). The lithologies were correlated in the understudy wells (Fig. 3 and Fig. 4).

Table 1: GR cut-off values for facies calculation.

Code	Lithology	GR
1	Shale	If>85
2	Shaly Sand	If between 50-85
0	Sand	If<50

The portion of the total void space of a porous material that is capable of transmitting a reservoir fluid is known as the Effective porosity ($\emptyset_e$). It happens when a fluid in a saturated porous media is unable to flow through all voids, but can flow through the voids that are interconnected. Dead-end pores are defined as unconnected pores. Occurrence of these dead-end pores are defined by particle size, shape, and packing arrangement (Gibb et al., 1984).

For calculation of effective porosity ($\emptyset_e$), (equations 1–5) are used. By substituting (equation 2 and 3 in equation 4), the neutron-density corrected porosity ($\emptyset_{ND}$) is calculated. Neutron porosity ($\emptyset_N$) is directly selected from the neutron log and density porosity ($\emptyset_D$) is calculated via (equation 1).

$$\emptyset_D = \frac{\rho_{ma} - \rho_b}{\rho_{ma} - \rho_f} \quad (1)$$

ρ_{ma} being the matrix density for sand at 2.65 g/cc, the bulk density of the formation compared to density log readings is identified as ρ_b while ρ_f is the flushed-water based mud apparent fluid density at 1.0 g/cc.

Permeability is considered as an important characteristic to understand the flow dynamics of the reservoir (Khan and Khan, 2018). The permeability of F2WC reservoir was estimated via Wyllie and Rose (1950) proposed equation (2), were Kw is the constan of Morris and Biggs (1967) and the parameters d and e are 6.0 and 2 respectively, as follows;

$$PERM = K_W \times \frac{PHI^d}{SW^e} \quad (2)$$

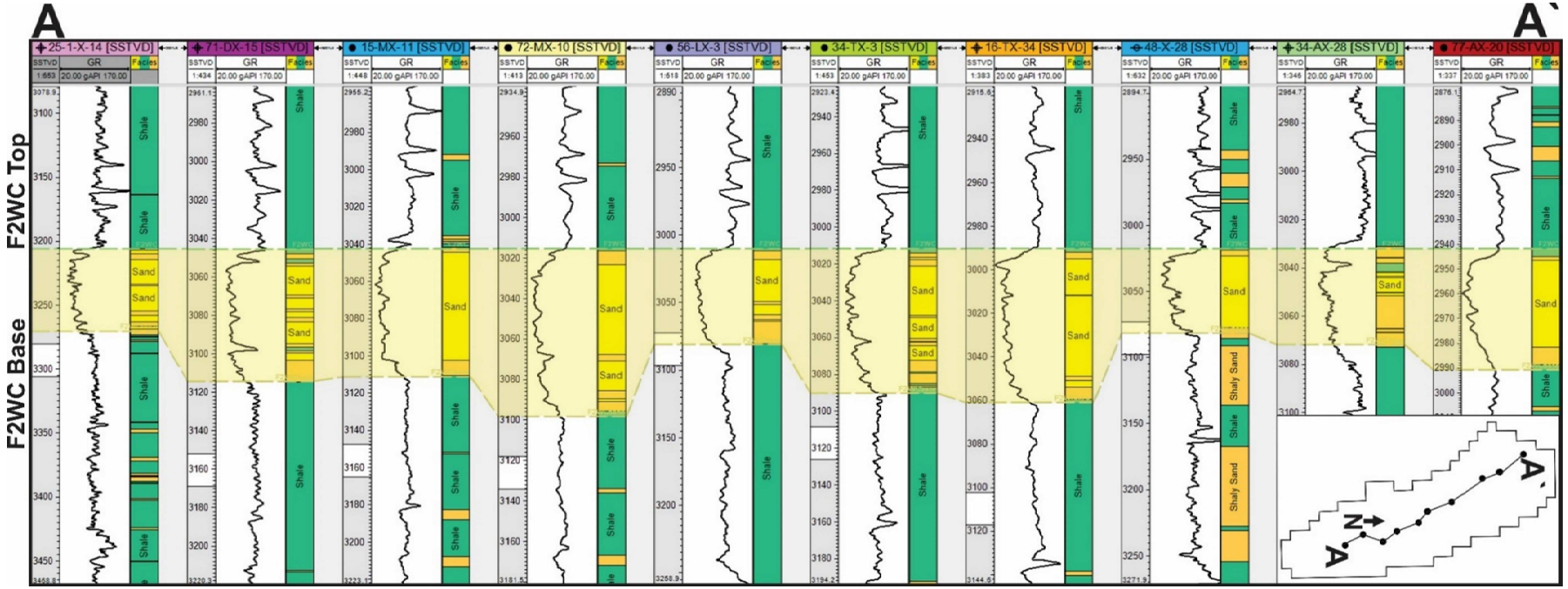

Figure 2: The first track represents the depth of the formation, second track shows the GR values of each formation, with drop change at the start of F2WC top. The highlighted yellow zone represents the F2WC sandstone with thickness variation. In the third track calculated facies from the stated cut-off has been represented, the cross-section follows the N-S trend from well (25-1-X-14 to 77-AX-20).

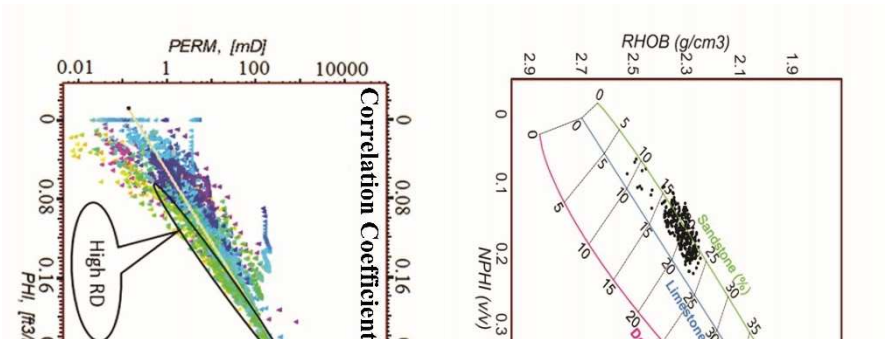

Figure 4: (A) ND cross-plot of F2WC where the clusters are falling near the sand zone envelop of standard plot (B)

Tri-plot of porosity, permeability and water saturation that represents an indication of low water saturation or high probability of hydrocarbon presence highlighted by black oval shape. (C) Tri-plot of porosity, permeability and deep resistivity validating the results by indicating a high resistivity of un-invaded zone which indicates a presence of hydrocarbon (D) Tri-plot of porosity, permeability and facies shows a gathering of clusters on the same location where high deep resistivity and low water saturation was found that indicates a good quality reservoir rock characteristic.

From Dewan (1983),

$$\emptyset_{Ne} = \emptyset_N - V_{sh} \times \emptyset_{Nsh} \quad (3)$$

$$\emptyset_{De} = \emptyset_D - V_{sh} \times \emptyset_{Dsh} \quad (4)$$

$$\emptyset_{ND} = \sqrt{\frac{\emptyset_{De}^2 + \emptyset_{Ne}^2}{2}} \quad (5)$$

$$\emptyset_e = \emptyset_{ND} * (1 - V_{sh}) \quad (6)$$

Here, $\emptyset_{Ne}$ is defined as the neutron shale corrected porosity while $\emptyset_{De}$ is the density shale corrected porosity. Volume of shale V_{sh} is estimated from the gamma ray log and $\emptyset_{Nsh}$= Neutron porosity and adjacent shale and $\emptyset_{Dsh}$= Density porosity in adjacent shale. Hurst and Archer (1986) proposed the equation (6) for estimating the shaly formations effective porosity.

Schlumberger (1975) equation (7) was used for the estimation of Water saturation (S_w). This equation (based on laboratory experiments and field experience) works well with formations having high shale contents (Asquit et al, 2004), they have no effect from the type of shale distribution rather if it is dispersed or laminated, equating as follows:

$$S_w = \frac{\sqrt{\left(\frac{V_{sh}}{R_{sh}}\right)^2 + \frac{\emptyset^2}{0.2 \times R_w \times R_t \times (1 - V_{sh})}} - \frac{V_{sh}}{R_{sh}}}{\frac{\emptyset^2}{0.4 \times R_w \times (1 - V_{sh})}} \quad (7)$$

Here, the shale volume fraction is represented as V_{sh} with the shale resistivity being R_{sh} and measured in (ohm-m). The $\emptyset$ being effective porosity fraction, resistivity of water at formation temperature (ohm-m) as R_w while R_t is the deep resistivity log reading (LLD) measuring the resistivity of the formation.

Neutron-Density cross-plot identifies the lithology of the target interval with clean quarzitic sand (as clusters fall in the region of sand). Cross-plots of porosity versus permeability with overlaid Z-values of facies and petrophysical properties reveal strong statistical relationships (correlation coefficient = 0.89) for the F2WC reservoir. Cross-plots were used here as tools to evaluate quality of the reservoirs. A high resistivity zone, which corresponds with clean sand and low water saturation, verifies the potential reservoirs. The F2WC cross-plot indicates a favorable hydrocarbon-bearing reservoir (Fig. 4).

3.2. **Basic Seismic Interpretation and Modelling**

Seismic to well tie is vital to commence basic seismic interpretation (Izadi et al. 2019). The synthetic seismograms for the time-domain correlation of the well tops with the seismic reflections (horizons) were developed. The synthetic seismogram of the well 67-1-TpX-10 and 25-1-X-14 (Fig. 5) were generated for the picking of seismic horizons. The specifications of both synthetic seismograms (Table 2) are a perfect fit without manual adjustments, only a shift was applied in both the synthetics to bring

them to their original positions. For confirmation, the horizons were further corroborated from published research (Cooper et al., 2003).

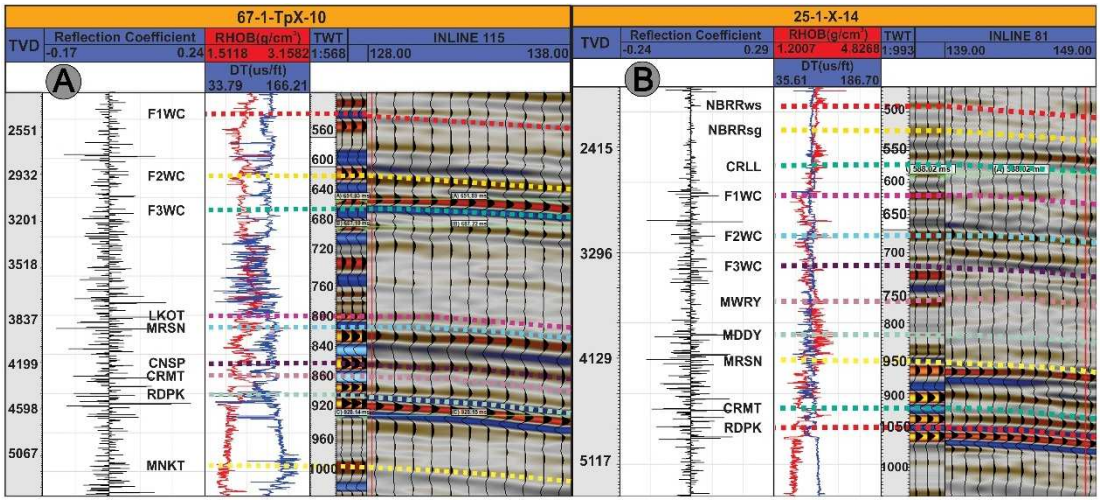

Figure 5: The synthetic consists of 6 tracks, from left to right, first track represents the depth in feet. The second track consists of the reflection coefficient and the third track is displaying the sonic and density log that are used in generation of reflection coefficient. However, the fourth track is representing the seismic time which can be compared to the depth, the fifth track consists of synthetic traces that are correlated with the adjacent seismic line displayed in the sixth track (A) Synthetic Seismogram 67-1-TpX-10, Inline 115 (B) Synthetic Seismogram 25-1-X-14, Inline 81.

Table 2: Synthetic Seismogram parameters.

Wavelet extraction	Ricker method
Location of extraction	67-1-TpX-10 / 25-1-X-14
Constant Phase	0
Wavelet length	100ms
Search Radius	100ft
Peak frequency	30 Hz
Sampling rate	2ms

The depth model was derived using the interval velocities of the formations (Table 3 and Table 4). After the domain conversion (time to depth) the zonation and layering of the stacked stratigraphy was delineated within the studied area. The layering further breaks down the zone into several layers for better resolution of thin packages.

Table 3: Velocity Data from synthetic 25-1-X-4, (Dataset: DOE).

FORMATION	DEPTH (ft)	TIME (s)	AVG VEL	INT VEL	INT TIME	INT DEN (g/cm^3)

			(ft/s)	(ft/s)	(s)	
Niobrara White Specks	2080	0.241	10495.23	10816.34	0.131	2.49
1st Wall Creek	2789	0.372	10608.33	12401.16	0.069	2.47
2nd Wall Creek	3214	0.441	10887.14	11884.73	0.038	2.45
3rd Wall Creek	3440	0.479	10966.39	11358.88	0.048	2.46
Mowry Shale	3712	0.527	11002.08	10683.48	0.044	2.4
Muddy Sandstone	3946	0.57	10977.62	10538.38	0.028	2.38
Dakota Sandstone	4093	0.598	10957.14	11513.6	0.014	2.44
Morrison	4175	0.613	10970.08	11912.46	0.015	2.51
Morrison Dunes	4267	0.628	10993.25	12621.41	0.073	2.47
Chugwater/Crow Mtn	4727	0.701	11162.56	12455.29	0.015	2.32
Goose Egg	5448	0.796	11642.41	16841.98	0.036	2.77
Tensleep	5749	0.832	11865.88	16927.49	0.006	2.7
Tensleep B Dolomite	5802	0.838	11903.71	16342.59	0.01	2.62
Tensleep B Sandstone	5881	0.848	11954.34	16725.28	0.002	2.6

Table 4: Velocity Data from synthetic 67-1-X-10, (Dataset: DOE).

FORMATION	DEPTH (ft)	TIME (s)	AVG VEL (ft/s)	INT VEL (ft/s)	INT TIME (s)	INT DEN (g/cm^3)
Niobrara White Specks	1800	0.23	10802.11	10946.94	0.119	2.49
1st Wall Creek	2452	0.35	10851.47	12597.55	0.065	2.49
2nd Wall Creek	2862	0.415	11125.58	12145.34	0.039	2.45
3rd Wall Creek	3100	0.454	11213.65	11393.87	0.048	2.42
Mowry Shale	3374	0.502	11230.92	10771.99	0.043	2.31
Muddy Sandstone	3608	0.545	11194.36	10616.83	0.027	2.2
Dakota Sandstone	3750	0.572	11167.35	12057.14	0.013	2.43
Morrison	3831	0.586	11187.77	12582.82	0.033	2.59
Sundance	4038	0.618	11261.99	12730.8	0.051	2.51
Chugwater/Crow Mtn	4360	0.669	11373.05	12568.98	0.013	2.33
Goose Egg	5052	0.76	11838.69	17255.08	0.035	2.77
Tensleep	5356	0.795	12078.8	16800.84	0.006	2.67
Tensleep B Dolomite	5404	0.801	12112.5	19379.94	0.003	2.7
Tensleep B Sandstone	5435	0.804	12140.5	15379.19	0.011	2.53

Seismic interpretation involved the picking of horizons and conversion of the horizons into the surfaces that were later used to generate the structural models (Fig. 6) of the study area. The seismic modelling involves generation of depth horizons using time surfaces, which were generated using the interpreted formations (Villarreal et al. 2019). Prior to the generation of depth horizons, a velocity model is required. Later, the geostatistical properties populated between the given thickness. Figure 7 shows an uninterpreted section for line xline 149 and the same seismic profile depicting the picked horizons of the stratigraphic units of the understudy area. The basic seismic interpretation and modelling helps to develop geostatistical models which augment the knowledge about reservoir characteristics of F2WC.

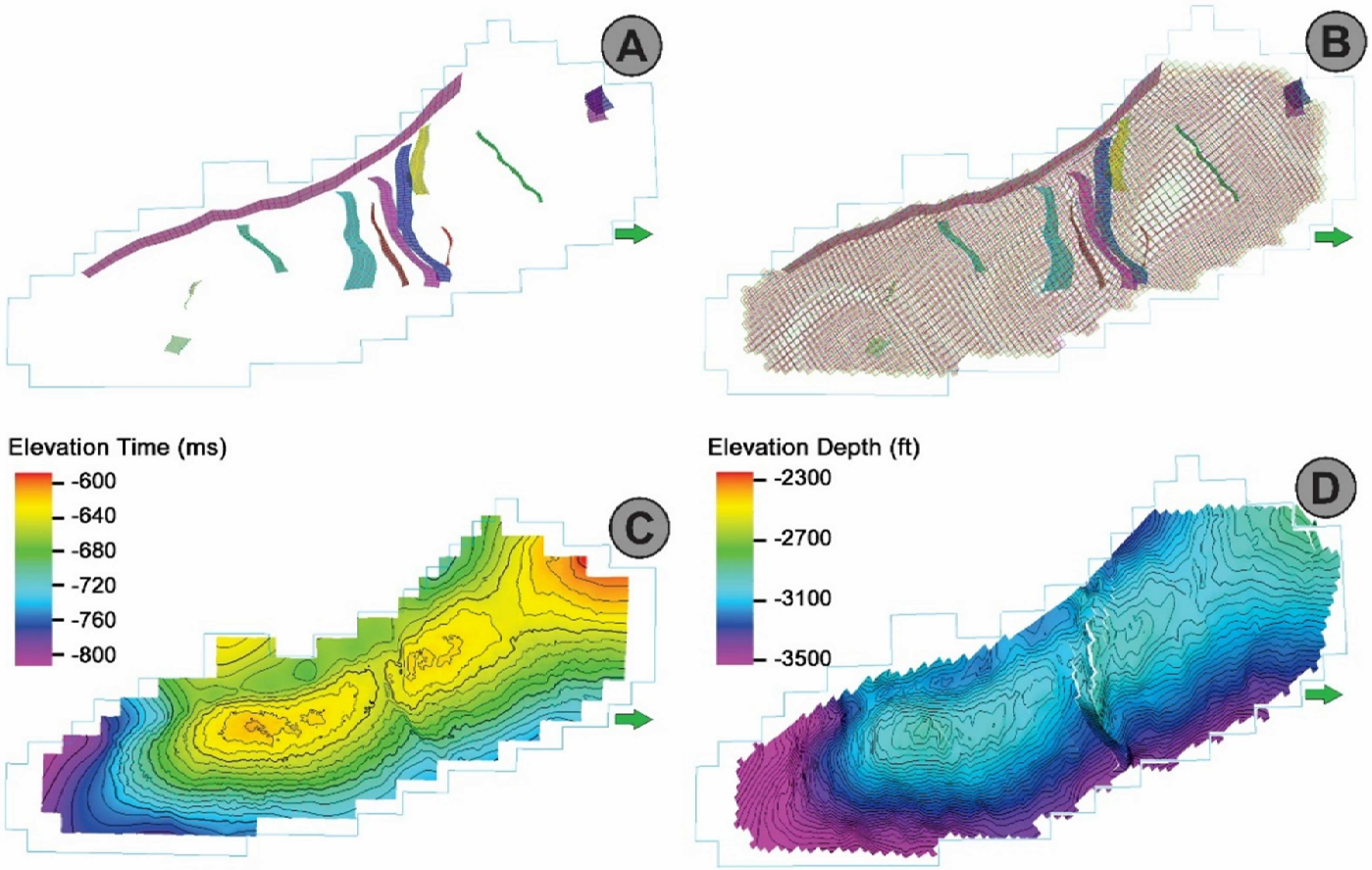

Figure 3: (A) Fault model of the F2WC at Teapot Dome representing the geometry and orientation of the major east-west trending faults and the basement fault running north-south. (B) Pillar gridding a grid size of 400x400 Skeleton, Top, Mid and Base, Teapot Dome. (C) Time surface of F2WC and which was generated following the picking of horizons using the synthetic seismogram (D) Depth surface of F2WC generated following the time-depth conversion.

A basic seismic model was defined within the function of Corner Point Gridding which enabled the application of fault modelling and pillar gridding. The function required interpretation of faults and fault sticks, the given dataset consisted of fault sticks which made it easier to model them, a fault model (Fig. 6A) of the teapot dome was generated using the fault sticks, this step enabled the option of gridding. Pillar gridding generated a skeleton of grids which were referred to as pixels that are used while modelling to fill in the properties. The fine gridding enabled higher resolution of the dataset but that came at the cost of higher data processing, for a basic model a grid size of 400x400 was perfect in this case. The grid generated a skeleton with all the fault geometries for top, mid and base (Fig. 6B). The next step of modelling involved generation of depth horizons using time surfaces, the surfaces were generated using the interpreted formations which were picked from 2D seeded picking (Fig. 6C). The depth horizon has been generated utilizing the time-depth relation developed utilizing Table 3 and 4.

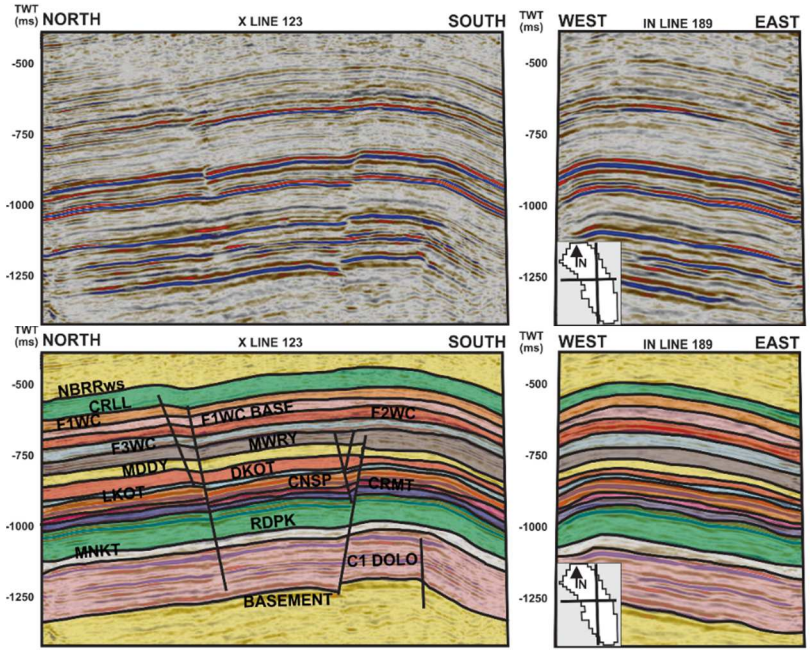

Figure 7: Uninterpreted and interpreted seismic section, X Line 149, IN Line 189. The area can be observed as a gentle domal structure which dips gently towards the north and east while the south and west dipping is steep. The major faulting can be observed on the northern flank which can also be observed in Fig. 6.

4. GEOSTATISTICAL EVALUATION

Geostatistical evaluation of reservoir is the most crucial step in modelling of thin packages (sand and shale) because it enhances the seismic resolution by integrating the petrophysical analysis. The geostatistical evaluation includes the verification of histogram and variogram of reservoir properties (porosity, permeability and water saturation). If the variation is high or the modeled values are different compared to the actual values (raw data), the model is unreliable.

Well logs are upscaled against their properties for the zones that have been created in the last step of seismic interpretation. These upscaled logs are then modelled after verifying with the variogram. There are various averaging methods each with their own pros and cons that includes the Arithmetic, Harmonic, Geometric, Root Mean Square, Median, Sum, Minimum, Maximum, Midpoint pick, Random pick and Zone specific.

All these methods can be further modified by changing the sampling method i.e., by treating them as points or lines, the samples can further be taken as simple, through the cell or by neighboring cell. The selection of the method depends upon the deviation of the averaged data from the raw data. With a variation greater than 5% the model ends up with having unrealistic values. The geometric averaging method and histogram (Fig. 8) helps in comparing the values of the original dataset from the well logs with the upscaled well logs and the calculated facies.

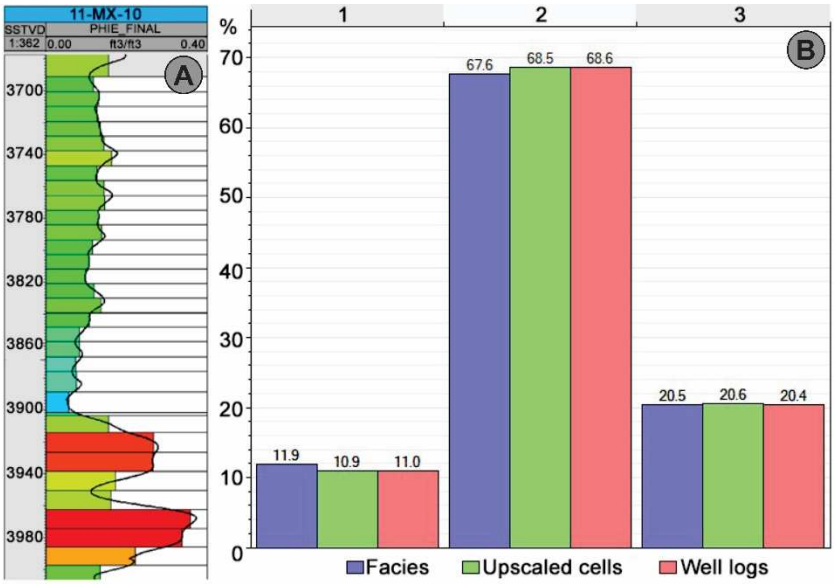

Figure 8: (A) Upscaled well log and (B) Histogram of well 11-MX-10 have been generated to validate the upscaled data with the raw log data.

A Variogram must be generated in order to build a correlation of the dataset by analysis of detailed spatial structure. It is used in the description of the spatial correlation followed by providing the lateral as well as the vertical ranges of the targeted intervals (Wang et al., 2013). While constructing a 3D geomodel, algorithms such as Sequential Gaussian Simulation (SGS), Sequential Indicator Simulation (SIS) and Truncated Gaussian simulation (TGS) are the inputs for the model variogram (Subyani, 2004). A variogram estimation can be followed as (equation 8):

$$\gamma(h) = \frac{1}{2N(h)} \sum_{i=1}^{N(h)} [x_i - y_i]^2 \qquad (8)$$

Here $N(h)$ is the pairs of points between data x_i and y_i that are separated by vector "h" known as (lag) meanwhile the location is known as "u". The degree of variability with reference to distance separation is denoted by variogram for semi-variance.

To define Variogram plotting the following parameters: (C) sill, (a) range and (C_0) nugget effect are required. The appearance and the behavior of the 3D geomodel that is being reproduced depends on the variogram. With a change in direction, the variogram and the values of parameters (Sill, range and nugget effect) change accordingly (Pawar, 2003). Anisotropic directions of sample data are defined as the major, minor and vertical axis (Fig. 9). Variogram model selection is a very delicate process, any wrong variogram selection affects on all of the other subsequent steps. Prior to 3D modeling validation of created modeled variogram is necessary.

Exponential, Gaussian and Spherical are the three variogram model types. A variogram constructed using the spherical type usually have a much better match with raw and upscaled well log. Calculations for the spherical model are done by taking the averages between the exponential and Gaussian models, making it suitable in most of the cases hence giving the advantage to the model type (Alfaaouri et al., 2009).

Mathematically a spherical variogram can be represented as;

If $h \leq a$

$$\gamma(h) = C_1[1 - \exp(-\frac{3h}{a})] \quad (9)$$

Otherwise

$$\gamma(h) = C_1 \quad (10)$$

Modelling variogram by using Equation (9) and (10) at shorter separation distance "h" creates a linear behavior that reaches the component of Sill which is spatially structured i.e. ($C_1 = C - C_0$) at range "a".

Therefore, determining the accurate anisotropy directions for the fitting procedure of model variogram is a most necessary step (Caers and Zhang, 2004). The variogram model and spherical variogram curve generated for F2WC has been illustrated in Figure. 9.

The results concluded from the study showed that the dome can be divided into Northern and Southern Blocks based on the major E-W trending fault that breaks the dome into two halves. The Southern Block is up-dip while the Northern block is downdip, this results into better reservoir properties on the Southern flank (Fig. 10). The high water-saturation, low porosity and low permeability on the northern flank is a result of the greater density of water compared to the oil and gas, and the compressional forces acting on the subducting flank respectively. For better visualization of the facies and reservoir property, F2WC has been modelled and shown on the x, y and z axis. The z-axis helps in the study of the lateral extent and variation of the facies and properties of each formation, while the x and y-axis helps in the study of the vertical extent and variation study of each formation. Each formation along with its properties has further been defined following each X, Y-axis (Fig. 11).

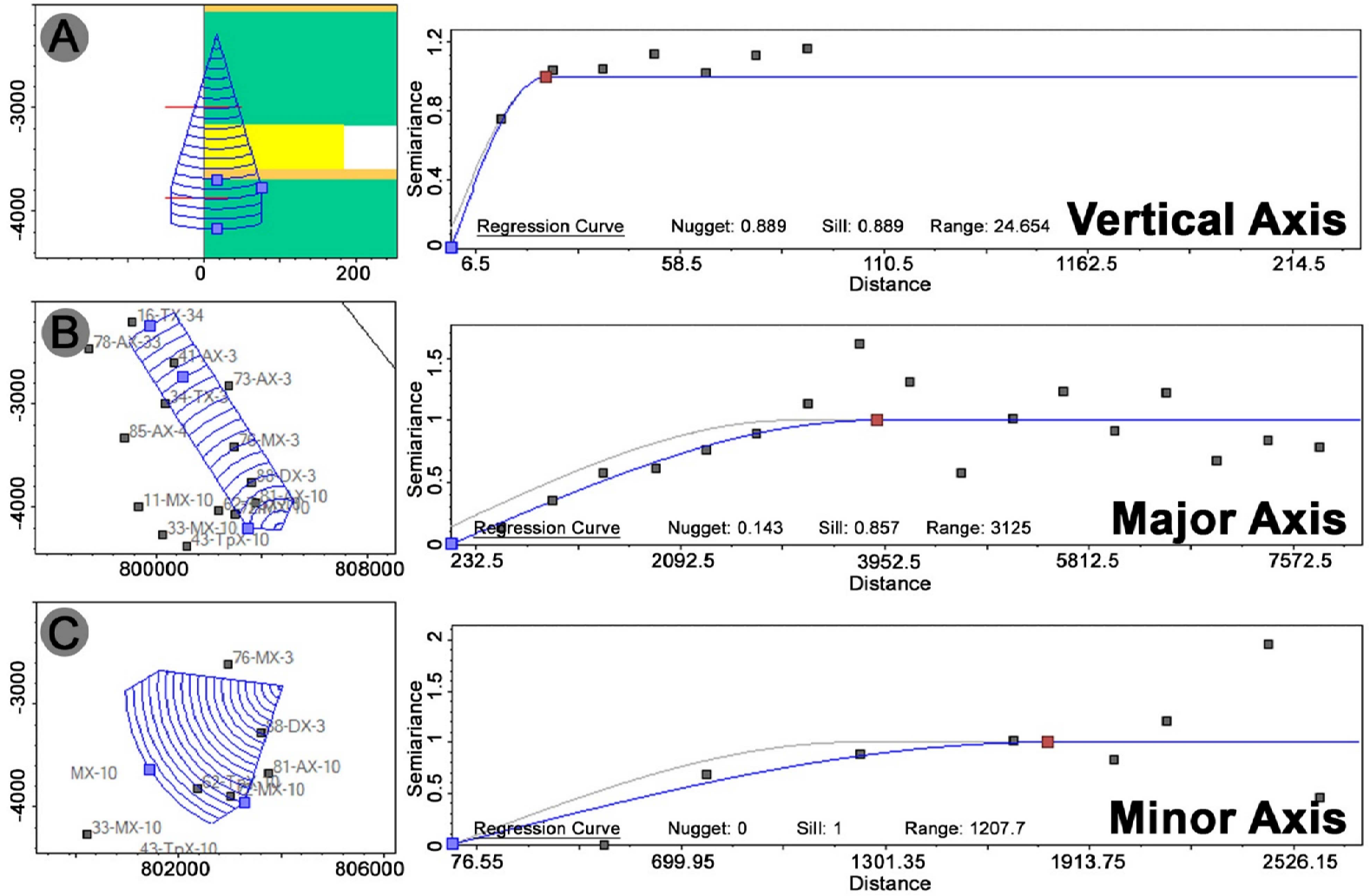

Figure 4: (A) Variogram Model of F2WC, Vertical Axis. (B) Variogram Model of F2WC, Major Axis and (C) Variogram Model of F2WC, Minor Axis. Model parameters [Structure Type- Spherical; Sill - 0.9999; Nugget – 0.01; Range (Major -3886.087, Minor- 1787.12, Vertical -24.334)].

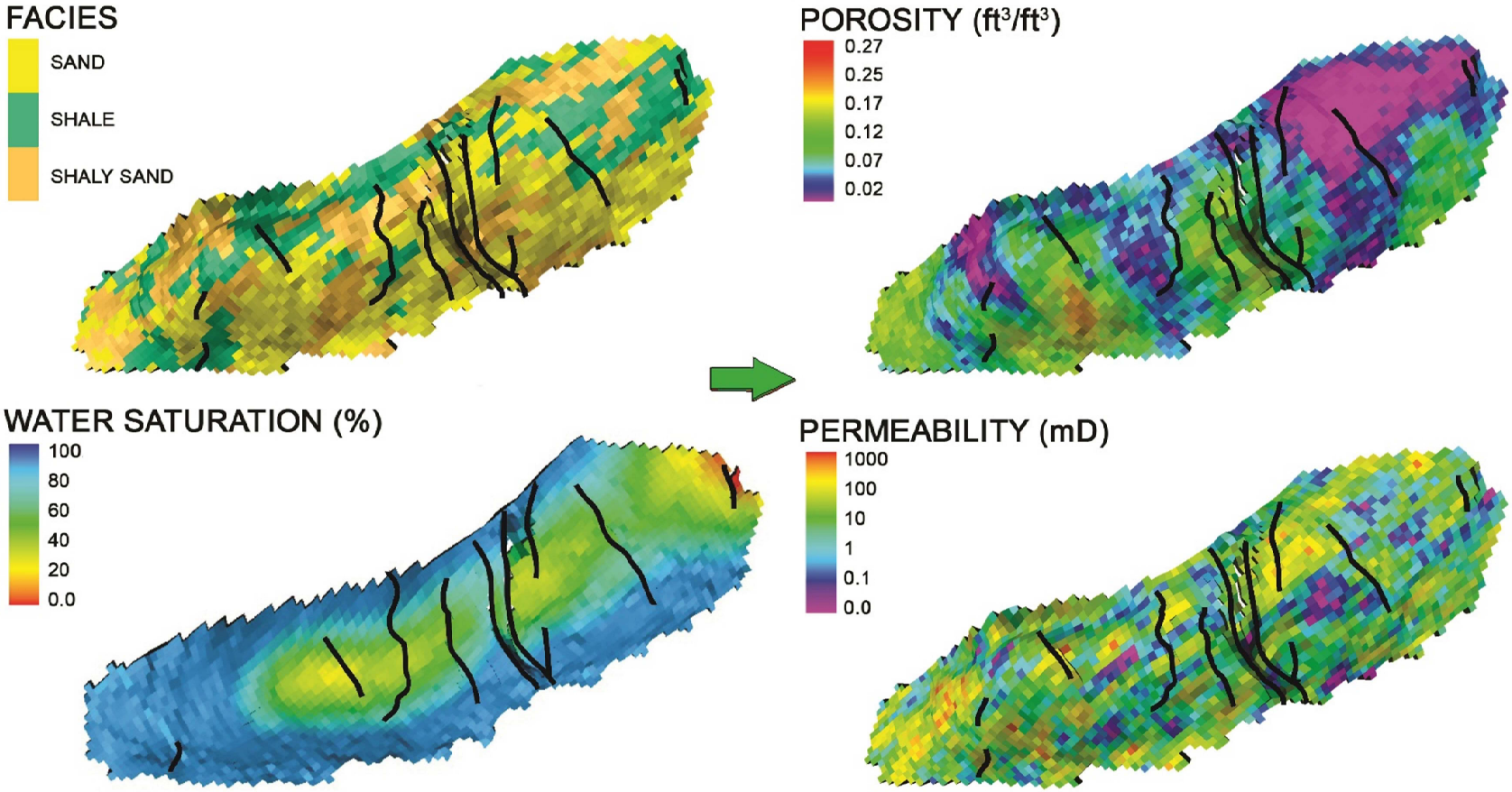

Figure 5: Facies model represents the three most important facies, i.e., the sand, shale, and shaly sand which were calculated utilizing the GR cut-off values (Table 1), Porosity model shows that even in a clean sand body the porosities are very low which gives us a hint to avoid those areas for exploration like the northern portion which can be compared with the Fig. 11. Water Saturation and Permeability models also play a vital role in targeting a potential prospect if you use the model and model cross-section (Fig. 11).

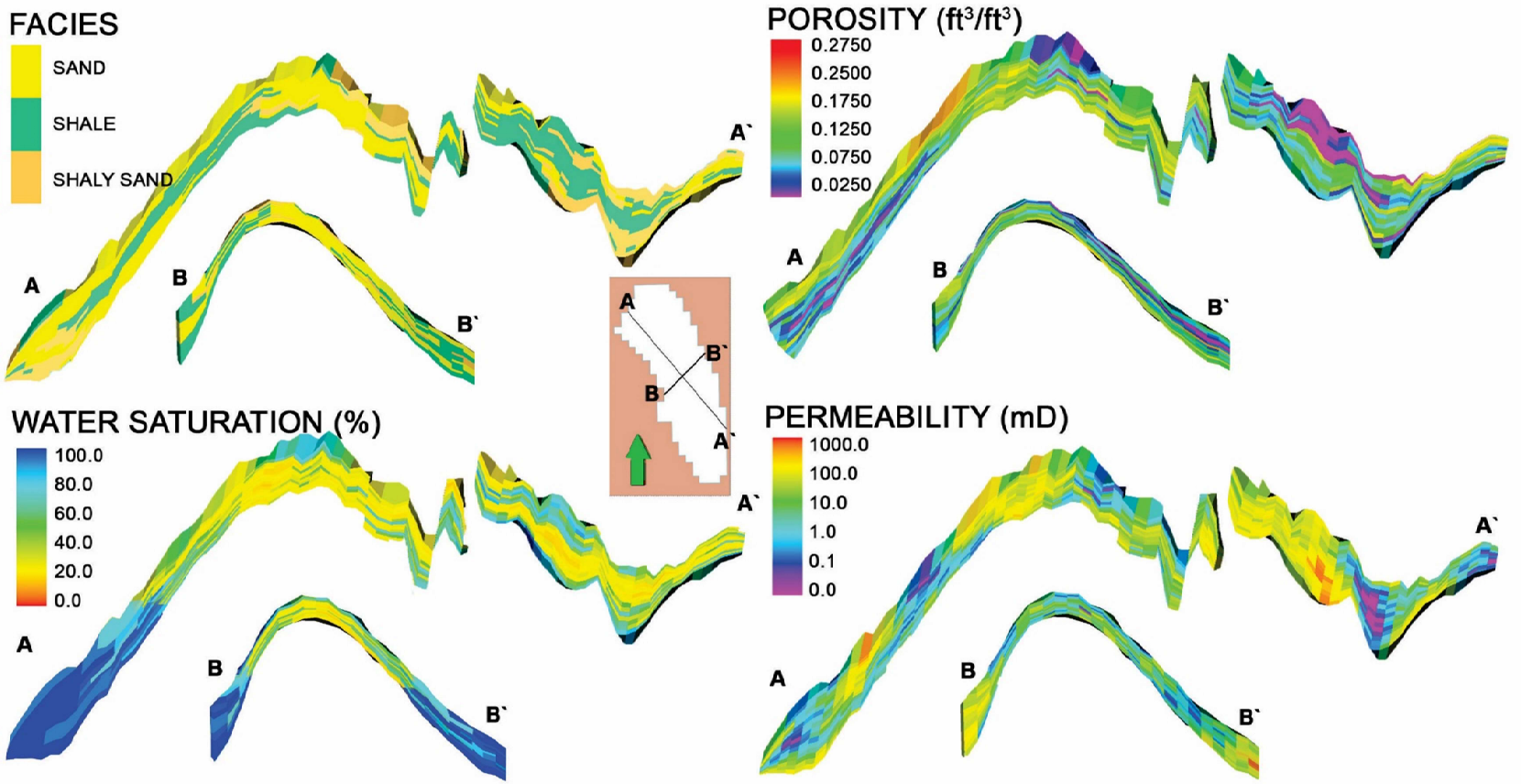

Figure 6: Facie, Permeability, Porosity and Water Saturation cross-section of Frontier 2nd Wall Creek Sandstone helps us to assess model. The suitable locations that are identified from Fig. 10 needs a cross check from this view to identify the lateral variation of the facies and properties.

The formation thicknesses are comparable to each other as no exaggeration has been applied on either of the axis. The comparison between the facies, porosity, permeability, and water saturation of the 3D geo-models shows us that all the reservoirs has a high percentage of shaly sand/shale and low porosity and permeability in the reservoirs, with high water saturations. The oil/water contact was not marked in this study. The F2WC reservoir has a small percentage of shaly-sand/shale and low water saturation, with high porosity and permeability. With average permeability readings between 0-100 mD, an average porosity of 18% and the average water saturation of 30%, F2WC is the most potential reservoir in the area. Understudied wells (utilized for the 3D model generation Fig. 10 and Fig. 11) of this case study suggested that the southern part of Teapot Dome is more prolific (based on Porosity, Permeability and water saturation) comparatively.

5. MODEL VALIDATION

Through blind well, the 3D models were validated in this study. The technique involves leaving out the one and/or more than one wells and later comparing the modeled curves with raw data (Hammad et al., 2010). Numerous realizations are necessary to achieve analogous results (Suleiman et al., 2012). The 72-MX-10 well was excluded from the modeling workflow and utilized as a blind well (Fig. 12). The reliability of the selected realization (base case) confirmed by comparing the blind well curves with the modeled reservoir properties (Fig. 12).

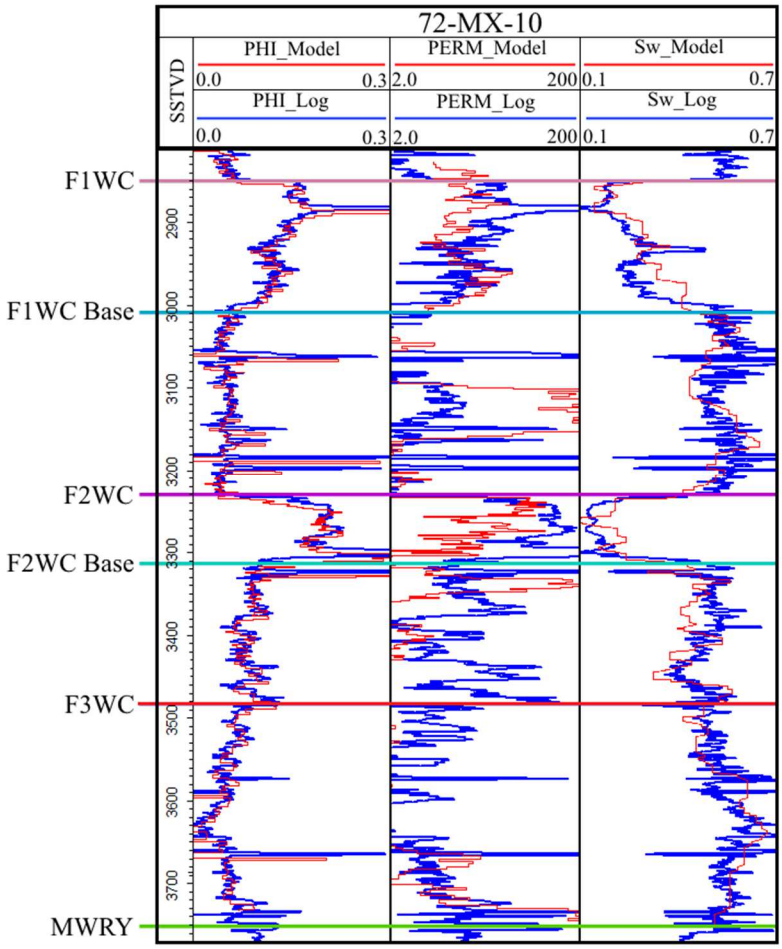

Figure 12: The blind well logs of porosity (1st tack), permeability (2nd Track) and water saturation (3rd track) shown by the blue color are perfectly fitting with red color curves of 3D modeled properties, demonstrates the stochastic algorithm robustness.

The base case of F2WC reservoir acquired after the simulations of 50 realizations of multivariate Monte Carlo method of property uncertainty. Pixel-based algorithm utilized for the F2WC reservoir modeling, which permits greater complexity and variability to portray the model uncertainty. Model uncertainty is the possible deviation from the original data, however in the presented case (Figure 11) the deviation is not more than 5% as witnessed in Figures 8a and 12.

Core data which is unfortunately not available for this study, considered as more reliable (higher accuracy compared to well log data) in depicting the true behavior of

the reservoir properties. For the further reservoir developments studies more control on spatially distributed results can be attained by tying modeled data with core data.

6. CONCLUSION

- Seismic interpretation alone cannot resolve the thin packages of F2WC. However, the petrophysical logs can probe into vertical resolution of the reservoir /stratigraphy encountered in the understudy wells.
- The integration of seismic data with well data in the form of 3D model improve lateral resolution which help to discriminate the F2WC by zonation and layering and model the reservoir characteristics (porosity, permeability, and water saturation) of thin facies distributed in F2WC.
- The southern part of Teapot Dome is more prolific (based on Porosity, Permeability and water saturation) comparatively.
- It is recommended that the proposed region of Teapot dome may be studied further to evaluate the reservoir potential of F2WC by geochemical analysis, core analysis and reservoir production data for uncertainty calculation of the proven field.

ACKNOWLEDGEMENT

The authors acknowledge the facility of Earth and Environmental Science DGDLab at BUKC. Authors also like to thank the potential reviewers for their critical review and suggestions to improve the manuscript. Last but not least, thanks to Department of Energy (DOE), USA for providing necessary data.

REFERENCES

Alfaaouri, S., Riahi, M., Alizadeh, N., and Rezae,i M., 2009. Permeability prediction in an oil reservoir and construction of 3D geological model by stochastic

approaches. Journal of Applied Sciences 9, 2016-2030. DOI: 10.3923/jas.2009.2016.2030.

Asquith, G., and Krygowski, D., 2004. Basic well log analysis: AAPG methods in exploration series 16, The AAPG, Oklahoma. https://store.aapg.org/detail.aspx?id=707.

Beikman, H.M., 1962. Geology of the Powder River Basin, Wyoming and Montana, with reference to subsurface disposal of radioactive wastes, Open-File Report 62-7. https://pubs.er.usgs.gov/publication/ofr627.

Blakey, R., 2011. Colorado Plateau Geosystems, Inc. Reconstructing the Ancient EARTH. R. Blakey, Producer, & Colorado Plateau Geosystems, Inc. Retrieved May. https://www2.nau.edu/rcb7/index.html.

Caers, J., and Zhang, T., 2004. Multiple-point geostatistics: A quantitative vehicle for integrating geologic analogs into multiple reservoir models. AAPG Memoir 80, 383-394.

Cooper, S.P., Goodwin, L.B., and Lorenz, J.C., 2006. Fracture and fault patterns associated with basement-cored anticlines: The example of Teapot Dome, Wyoming. AAPG Bull 90, 1903-1920. Doi.org/10.1306/06020605197.

Cooper, S.P., Hart, B., Lorenz, J.C., Goodwin, L., and Milliken, M., 2002. Outcrop and seismic analysis of natural fractures, faults and structure at Teapot Dome, Wyoming, pp.63-74.

Craddock, W.H., Drake, R.M., II, J.C., Merrill, M.D., Warwick, P.D., Madalyn, S., Blondes, M.A.G., Freeman, P.A., Cahan, S.M., DeVera, C.A. and Lohr, C.D., 2012. Geologic Framework for the National Assessment of Carbon Dioxide Storage Resources: Powder River Basin, Wyoming, Montana, South Dakota, and Nebraska. US Department of the Interior, US Geological Survey. Geological Survey Open-File Report 2012–1024–B, pp.30. https://pubs.usgs.gov/of/2012/1024/b/

Craig, L., 1972. Mississippian system in: Geologic Atlas of the Rocky Mountain Region: Denver, Colorado. W. W. Mallory, ed. Rocky Mountain association of Geologists pp.100-110. http://store.aapg.org/detail.aspx?id=1169

Curry, W.H., 1977. Teapot Dome—Past, Present, and Future. AAPG Bull 61, 671-691.

Darcy, H.P.G., 1856. Les Fontaines publiques de la ville de Dijon. Exposition et application des principes à suivre et des formules à employer dans les questions de distribution d'eau, etc. V. Dalamont.

Dewan, J.T., 1983. Essentials of modern open-hole log interpretation. PennWell Books.

Dolton, G.L., & Fox, J.E., 1995. Powder River Basin Province (033). DL Gautier, GL Dolton, KI Takahashi, and KL Varnes, eds.

Gibb, J.P., Barcelona, M.J., Ritchey, J.D., and LeFaivre, M, H., 1984. Effective porosity of geologic materials: First annual report, Report, Illinois State Water Survey. https://www.ideals.illinois.edu/handle/2142/73188

Hammad, M., Shahlol, A., Hajaj, S., Aoues, A., El Werfali, H., BuArgoub, F., Kirkham, A.J.f.b., 2010. Seismically driven characterization of vuggy porosity and fractures in a carbonate field, Sirte Basin, Libya. 28.

Houston, R., 1993. Late Archean and early Proterozoic geology of southeastern Wyoming. Geology of Wyoming: Geological Survey of Wyoming Memoir 5, pp.78-116.

Hurst, A., and Archer, J., 1986. Sandstone reservoir description: An overview of the role of geology and mineralogy. Clay Minerals 21, 791-809.

Izadi, H., Innanen, K.A., Lamoureux, M.P.J.J.o.A.G., 2019. Local signal regularity and smoothness as a means for seismic Q estimation. 170, 103853.

Khan M. J., and Khan H. A., 2018. Petrophysical Logs Contribute in Appraising Productive Sands of Lower Goru Formation, Kadanwari Concession, Pakistan. J. of Petr. Exp. and Production Tech., 8 (4), 1089–1098,

Lageson, D.Ra., and Spearing, D.R., (editors) 1991. Roadside Geology of Wyoming. Missoula, Montana, Mountain Press Publishing Co., second edition: pp.271.

Love, J.D., Christiansen, A.C., and Ver Ploeg, A.J., 1993. Stratigraphic chart showing Phanerozoic nomenclature for the State of Wyoming: Wyoming Geological Survey Map Series 41. https://www.wsgs.wyo.gov/wyoming-geology/stratigraphy.

Morris, R., Biggs, W., 1967. Using log-derived values of water saturation and porosity, SPWLA 8th Annual Logging Symposium. Society of Petrophysicists and Well-Log Analysts.

Pawar, R.J., 2003. Introduction to geostatistics. In Developments in petroleum science 51, pp.85-95. Los Alamos National Laboratories, Los Alamos, NM, USA. Elsevier.

Payne, A.A., and Saffer, D.M., 2005. Surface water hydrology and shallow groundwater effects of coalbed natural gas development, upper Beaver Creek drainage, Powder River Basin, Wyoming. Western Resources Project Final Report—Produced Groundwater Associated with Coalbed Natural Gas Production in the Powder River Basin. Wyoming State Geological Survey Report of Investigations 55, pp.5-43. http://webcache.googleusercontent.com/search?q=cache:K-cSsJ4wdgUJ:www3.geosc.psu.edu/~dms45/CBM_report.pdf+&cd=1&hl=en&ct=clnk&gl=pk.

Peterson, J., 1972. Jurassic system. Geologic Atlas of the Rocky Mountain Region: Denver, Colorado, Rocky Mountain Association of Geologists, 331. https://www.abebooks.com/Geologic-Atlas-Rocky-Mountain-Region-United/18716435796/bd.

Picard, M.D., Snoke, A., Steidtmann, J., and Roberts, S., 1993. The early Mesozoic history of Wyoming. Geology of Wyoming: Geological Survey of Wyoming Memoir 5, pp.211-248.

Schlumberger, A., 1975. Guide to wellsite interpretation of the Gulf Coast. Schlumberger Well Services, Houston. https://books.google.com.pk/books/about/A_Guide_to_Well_Site_Interpretation_for.html?id=ujt8tAEACAAJ&redir_esc=y.

Subyani, A.M., 2004. Geostatistical study of annual and seasonal mean rainfall patterns in southwest Saudi Arabia. HYDROLOG SCI J 49, 803-817. Doi/abs/10.1623/hysj.49.5.803.55137.

Villarreal, O., León-López, K., Espinosa, D., Agudelo, W., Arguello, H.J.J.o.A.G., 2019. Seismic source reconstruction in an orthogonal geometry based on local and non-local information in the time slice domain. 170, 103846.

Walker., R.G., and Bergman, K.M., 1993. Shannon Sandstone in Wyoming: a shelf-ridge complex reinterpreted as lowstand shoreface deposits. J SEDIMENT PETROL 63, 839–851. DOI: 10.1306/D4267C21-2B26-11D7-8648000102C1865D.

Wang, X., Sain, K., Satyavani, N., Wang, J., Ojha, M., and Wu, S., 2013. Gas hydrates saturation using geostatistical inversion in a fractured reservoir in the Krishna–Godavari basin, offshore eastern India. MAR PETROL GEOL 45, 224-235. Doi.org/10.1016/j.marpetgeo.2013.04.024

Watson, J.E., 1980. Catalog of Wyoming Stratigraphy. Tooke Engineering. https://www.worldcat.org/title/catalog-of-wyoming-stratigraphy/oclc/7835265.

Wyllie, M., Rose, W.D.J.J.o.P.T., 1950. Some theoretical considerations related to the quantitative evaluation of the physical characteristics of reservoir rock from electrical log data. 2, 105-118.

Association, W.G., 2000. Wyoming Oil and Gas Fields Symposium: Powder River Basin. The Association.